Philbert, S. A., Xu, J., Unwin, R. D., Dowsey, A. W., & Cooper, G. J. S. (2021). Widespread severe cerebral elevations of haptoglobin and haemopexin in sporadic Alzheimer's disease: Evidence for a pervasive microvasculopathy. *Biochemical and Biophysical Research Communications*, *555*, 89-94. https://doi.org/10.1016/j.bbrc.2021.02.107

Widespread severe cerebral elevations of haptoglobin and haemopexin in sporadic Alzheimer's disease: evidence for a pervasive microvasculopathy

Sasha A. Philbert [a, b], Jingshu Xu [a, b, c], Richard D. Unwin [a, b], Andrew W. Dowsey [a, b, d], Garth J.S. Cooper [a, b, c,*]

[a] *Division of Cardiovascular Sciences, School of Medical Sciences, Faculty of Biology, Medicine and Health, The University of Manchester, Manchester, M13 9WL, UK*

[b] *Centre for Advanced Discovery and Experimental Therapeutics (CADET), Manchester Academic Health Sciences Centre, Manchester, UK*

[c] *School of Biological Sciences, Faculty of Science, University of Auckland, Private Bag 92 019, Auckland 1142, New Zealand*

[d] *Department of Population Health Sciences and Bristol Veterinary School, Faculty of Health Sciences, University of Bristol, Bristol BS8 2BN, UK*

* Corresponding author: School of Biological Sciences, University of Auckland, Private Bag 92 019, Auckland 1142, New Zealand; E-mail address: g.cooper@auckland.ac.nz (G.J.S. Cooper).

Abbreviations: AS, arteriosclerosis; BBB, blood-brain barrier; CAA, cerebral amyloid angiopathy; CB, cerebellum; CG, cingulate gyrus; ENT, entorhinal cortex; fc, fold-change; FDR, false-discovery rate; iTRAQ, isobaric tags for relative and absolute quantitation; LC, liquid chromatography; LH, lipohyalinosis; MCX, motor cortex; PMD, post-mortem delay; SCX, sensory cortex; sAD, sporadic Alzheimer's disease

Abstract

Sporadic Alzheimer's disease (sAD) is the commonest cause of age-related neurodegeneration but there are no available treatments with demonstrated disease-modifying actions. It is therefore relevant to study hitherto-unknown aspects of brain structure and function to seek new disease-related mechanisms that might be targeted by novel disease-modifying interventions. During hypothesis-generating proteomic investigations in a case-control study of sAD, we observed widespread elevations of haptoglobin and haemopexin in all six brain-regions studied, which together represent much of the brain. Measured perturbations were significant, with the posterior probability of upregulation generally >95% and haptoglobin doubling in expression levels on average across deep brain structures (hippocampus, entorhinal cortex and cingulate gyrus) as well as sensory and motor cortices, and cerebellum. Haptoglobin and haemopexin are often regarded as circulating proteins whose main functions are to bind, respectively, the strongly pro-inflammatory extracellular haemoglobin and haeme molecules that form following haemolysis, thereby promoting their clearance and suppressing damage they might otherwise cause, for example, acute kidney injury. To our knowledge, elevations in neither cerebral haptoglobin nor haemopexin have previously been linked to the pathogenesis of sAD. *Post-mortem* examination of these cases showed no signs of macroscopic cerebral haemorrhage. These findings demonstrate pervasive cerebral elevation of haptoglobin and haemopexin, consistent with low-level intracerebral leakage of haemoglobin and consequent haeme formation throughout sAD brain. They point to a widespread underlying microvasculopathy that facilitates erythrocyte leakage, thereby triggering elevated tissue-free haemoglobin and driving the measured elevations in haptoglobin and haemopexin.

Keywords

Sporadic Alzheimer's disease; Brain glucose; Cerebral haptoglobin; Cerebral haemoglobin; Cerebral microvasculopathy; Blood-brain barrier leakage

1. Introduction

Sporadic Alzheimer's disease (sAD) is the most common cause of age-related neurodegeneration and dementia [1,2], with many millions of people currently affected worldwide [3]: by contrast, familial Alzheimer's disease is a rare autosomal dominant condition. The cause of sAD is unknown, possibly because it is heterogeneous and caused by interactions of ageing with various other risk factors [2]. Its course displays clinically-insidious onset with progressive decline in neurocognitive function. Pathological signs include cerebral plaques comprising amyloid β (Aβ) protein, tangles comprising hyperphosphorylated tau (τ) protein [4], and localized defects in cerebral-glucose uptake demonstrable by brain imaging with 2-deoxy-2-[^{18}F]-fluoro-D-glucose positron emission tomography (FDG-PET) [5]. Recently, marked elevations in glucose levels of sAD brain have been reported by three independent groups [6-8]. The evident global perturbation of key metabolites related to energy metabolism supports the notion of sAD as a pervasive metabolic disorder [9]. How these metabolic defects relate to the Aβ and τ perturbations in the cytotoxic processes that lead to or cause neurodegeneration and dementia is not entirely clear, but linking mechanisms may involve insulin resistance [10], elevated glucose [6,9] and/or vitamin B5 deficiency [11] of the brain.

There is a high rate of failure in AD drug-development programmes, and strategies aimed at modifying protein aggregation (that is, of Aβ or τ) have not, to date, succeeded in producing therapeutic interventions with disease-modifying properties [12].

The slowly progressive cerebral lesions of sAD include pathological protein aggregates, loss of neurons and synapses, alterations in immunological processes [13,14], inflammation, and signs of defects in cerebral-glucose uptake and the central pathways of fuel metabolism [5,6,9]. Extracellular Aβ accumulation occurs in the brain parenchyma as diffuse, focal or stellate deposits, and may also involve the vessel walls of arteries, veins and capillaries [13,14]. The progression of τ pathology is stepwise and stereotyped, passing from the entorhinal cortex (ENT), through the hippocampus (HP) to the isocortex [14]. The pattern of neuronal loss is heterogeneous and area-specific, and its mechanism remains uncertain [14].

An increasing number of studies suggest a vascular contribution to the pathobiology of sAD [15], which is often accompanied by vascular changes including cerebral amyloid angiopathy (CAA),

[1,13,14] and mixed arteriosclerosis/lipohyalinosis (AS/LH) [1]. In one neuropathological study, the first stage of CAA involved leptomeningeal and isocortical microvessels; the second was characterized by additional Aβ deposition in allocortical and midbrain vessels; and in the third, CAA was observed in the basal ganglia, thalamus, and lower brainstem [1]. By contrast, AS/LH initially affects the basal ganglia; then spreads into the deep white matter, the leptomeningeal arteries of the cortex, the cerebellum, and the thalamus; and finally into the brainstem vessels.

Here we applied liquid chromatography (LC)-mass spectrometry-based proteomics [16] to relatively quantify protein concentrations in brain tissue in six representative regions from nine sAD cases and nine matched controls. We analysed 18 human brains with short *post-mortem* delays wherein six anatomically- and functionally-distinct brain regions were examined, of which three are known to undergo severe neuronal damage in sAD (ENT; HP; and cingulate gyrus, CG); two to be moderately affected (sensory cortex, SCX; and motor cortex, MCX); and one (cerebellum, CB) said to be relatively spared [17,18]. We applied mixed hypothesis-generating and pathway-targeted methodologies with Bayesian modelling to quantitate case-control differences in brain levels of nine haemoglobin/iron-relevant proteins. Analysed proteins were: haptoglobin; haemopexin; haemoglobin; (three chains: α, β and δ); fibrin (three fibrinogen chains: α, β and γ); haeme oxygenase-2; high-affinity haemopexin-haeme-complex receptor (lipoprotein receptor-related protein/cluster of differentiation 91, LRP1/CD91); biliverdin reductases (A and B); ferritin (light- and heavy-chains); and transferrin; comprising 15 proteins in all. Total brain-iron values were measured in the same six regions.

2. Methods

The general methods employed in this study of *post-mortem* human brain from sAD cases and controls were as previously described [16,19,20]: salient aspects are briefly summarised in the Methods section and in greater detail in the Suppl. Methods and, where indicated, in referenced prior publications. Methods specific to the current study are described in sufficient detail to enable their repetition when taken together with previous descriptions [16,21].

2.1. Ethics and acquisition of human brains

Experiments were performed at the Universities of Auckland and Manchester, consistent with relevant local and national human ethics regulations and applicable guidelines. This study of *post-mortem* brain was approved by the University of Auckland Human Participants Ethics Committee with informed consent from all families.

Human brains were obtained from the Neurological Foundation Human Brain Bank, University of Auckland, as previously described [16,19].

2.2. Brain dissection, sample acquisition and histopathological diagnosis

Brains were dissected as described (Suppl. Methods). Cases had *ante-mortem* clinical evidence of dementia whereas controls, selected by matching for age, sex and *post-mortem* delay (PMD), did not (Table 1; Suppl. Table 1). PMD was generally short in both cases and controls. Aliquots of grey matter were dissected from six regions: ENT, HP, CG, SCX, MCX, and CB.

Aliquots of 100 ± 5 mg wet-weight were dissected from each region, stored at -80 ^{o}C until analysis, and otherwise treated as described [19].

A consultant neuropathologist diagnosed or excluded sAD by applying the Consortium-to-Establish-a-Registry-for-Alzheimer's-Disease (CERAD) criteria [22], and determined the neuropathological severity by assigning the Braak stage [17], and amyloid load by applying the 2013

consensus National Institute on Aging–Alzheimer's Association guidelines [16,23]. Grouped case data are shown in Table 1, and individual case data in Suppl. Table 1.

One control patient had neuropathological findings consistent with sAD (Braak Stage II) and was therefore diagnosed with preclinical disease but retained in the analysis: this finding is consistent with the known frequency of presymptomatic sAD in similarly aged groups in the study population.

[Table 1 here]

2.3. Protein extraction and preparation for iTRAQ labelling.

Protein extraction and preparation for iTRAQ protein relative quantitation was performed as previously described with each brain region analysed independently [16]. Detailed descriptions of the methodology are presented in the Suppl. Methods.

2.4. Low-pH LC-mass spectrometry data acquisition

Data acquisition by LC-mass spectrometry was performed as previously described [16] and detailed in the Suppl. Methods.

2.5. Brain-iron levels

Total brain-iron levels were measured by inductively-coupled plasma mass spectrometry using published, validated methods [21,24].

2.6. Data processing

The data-processing methodologies applied in this study are generally as previously described [16] and are otherwise as detailed in the Suppl. Methods. Proteins relevant to the underlying experimental hypothesis were identified by the authors' prior field-related knowledge of relevant protein pathways as listed in the Introduction, and were assessed by Bayesian probability distribution plots for each protein, along with probability distribution plots for each case, by application of data available at: www.manchester.ac.uk/dementia-proteomes-project [16]. We defined significance using a local FDR threshold of 10%.

2.7. Data availability

All fully-processed data used in this case-control study are available via the Supplementary Data associated with our previous article and online in a searchable format, along with probability distribution plots for each protein at: www.manchester.ac.uk/dementia-proteomes-project [16].

3. Results and Discussion

Here we report measurements of nine proteins of the haemoglobin/haeme/iron regulatory pathways and of total brain iron, in tissues from six brain regions in nine cases of sAD, and nine matched controls. Study-group characteristics are summarized in Table 1, and individual patient data are shown in Suppl. Table 1.

Here, expression probability distributions of haptoglobin and haemopexin in six brain regions are shown in Fig. 1 and the corresponding Bayesian differential quantification data in Table 2. The different components of an exemplary expression probability distribution diagram are shown for guidance in Suppl. Fig. 1. Each data plot shows the probability distribution along with the most likely mean-expression ratio and the calculated local false-discovery rate (FDR; 1 – posterior probability) for each molecule that had a differential expression between cases and controls of at least 5%. Suppl. Fig. 2 & 3 show the Bayesian probability distributions for estimated levels of haptoglobin and haemopexin in each individual sample in this study with respect to the mean-control level.

These data provide robust evidence for substantive, clinically-relevant increases in levels of haptoglobin and haemopexin in all six brain regions from the nine sAD cases studied. Haeme released from haeme-binding proteins by internal haemorrhage, haemolysis or myolysis, is highly toxic due to oxidative and proinflammatory effects [25]. Expression of haptoglobin and haemopexin can be upregulated by increases in their respective binding partners, free haemoglobin and free haeme, whose toxic properties they suppress when bound. We could find no available reports to suggest that such elevations in cerebral haptoglobin and haemopexin could be caused by alternative mechanisms other than those described here.

Therefore, these data show that increased amounts of free haemoglobin and free haeme were widespread throughout the brain in all cases when elevations of haptoglobin and haemopexin levels were elicited. Patients with sAD are not known to develop systemic haemolysis or elevations in plasma levels of haptoglobin or haemopexin, so the observed changes are probably limited to the brain. There is also evidence that both haptoglobin [26] and haemopexin [27] can be produced by brain cells.

[Fig. 1 here]

We interpret these data as consistent with the idea that haptoglobin and haemopexin are produced in the sAD brain in response to the presence of free haemoglobin and free haeme in the brain substance caused by ingress of erythrocytes following vascular damage. Free haemoglobin and free haeme are likely to occur in the brain through infiltration of erythrocytes and subsequent intracerebral haemolysis, causing the extravasation of these substances via a process similar to that which occurs, for example, in diabetic neuropathy [28]. These findings imply the existence of a pervasive microvasculopathy in sAD, which compromises the integrity of blood-vessel walls sufficiently to permit the passage of erythrocytes (average diameter ~8 μm) from the vascular lumen across the capillary wall.

Finally, it is important to observe that none of the sAD cases showed any macroscopic or microscopic evidence of haemorrhage detectable at *post-mortem* examination (Suppl. Table 1); rather, all cases clearly meet the criteria for diagnosis of sAD. Therefore, the observed increases in haptoglobin and haemopexin in these cases did not represent responses, for example, to occult subarachnoid haemorrhage, in which haptoglobin levels undergo a brief compensatory increase followed by a decrease due to the removal of haptoglobin-haemoglobin complexes [29].

[Table 2 here]

We also measured the regional brain levels of α, β and δ subunits of haemoglobin (Suppl. Table 2 & Suppl. Fig. 4). There was modest evidence for increased levels of all three haemoglobin subunits in the ENT, but nowhere else. The ENT is often said to be the most heavily-damaged region in the sAD brain, so these data could indicate that erythrocyte leakage may proceed at a faster pace there than elsewhere, causing modest haemoglobin accumulation. Taken together, these data suggest prior elevation of free cerebral haemoglobin levels, but not enough to overwhelm the haptoglobin/haemopexin scavenger systems, as indicated by the lack of haemoglobin accumulation in all but the ENT, where there is evidence for only modest accumulation.

We found that elevations in cerebral levels of the three fibrinogen chains provides evidence for widespread leakiness of the blood-brain barrier (BBB) in sAD (Suppl. Table 3; Suppl. Fig. 5). Following vascular injury, the preproproteins of each fibrinogen chain are proteolytically processed by thrombin (EC 3.4.21.5) during the conversion of fibrinogen to fibrin. Histologically-demonstrated

accumulation of fibrin in the peri-vascular space around microvessels is a diagnostic test for leakiness of the BBB in cerebral sections, but direct protein-level evidence for accumulation of fibrin in the brain in sAD has hitherto been lacking. Here, we found that levels of all three fibrinogen chains, α, β and γ, were substantively elevated in all brain regions, providing very strong evidence for a widespread process causing leakiness of the BBB in sAD (Suppl. Table 3; Suppl. Fig. 5). Whether BBB leakiness is caused by the same process that provides a route for erythrocytes to cross into the brain substance requires clarification. These findings provide strong molecular evidence for widespread vascular injury in all sAD cases studied here, and present a proteomics-based assay for BBB leakage that can act as an alternative for the histological test, if required.

Levels of LRP1/CD91, the haemopexin-haeme complex receptor, showed no evidence of differing between cases and controls (Suppl. Table 4; Suppl. Fig. 6). We conclude that levels of LRP1/CD91 are sufficient to mediate the clearance of haemopexin-haeme complexes from the sAD brain without the necessity for its induction, given the relatively low rates of erythrocyte leakage imputed from these data.

Haeme oxygenase (HMOX; EC 1.14.99.3) is an essential enzyme of haeme clearance and catabolism that cleaves haeme to biliverdin. HMOX activity is induced by its substrate haeme and by various non-haeme moieties. There are two HMOX isozymes in man that belong to the haeme oxygenase family: the inducible HMOX-1 and the constitutive HMOX-2. *In vivo* deletion of HMOX-2 disables execution of the acute inflammatory and reparative response after epithelial injury and can cause an exaggerated inflammatory response in certain diseases. We readily quantitated HMOX-2 in all subjects from all six brain regions (Suppl. Table 5; Suppl. Fig. 7) whereas no signal from HMOX-1 was detected, either because HMOX-1 was not present or below the limit of detection. We found moderate evidence for decreased HMOX-2 levels in the ENT and CG.

After the cleavage of haeme, biliverdin reductase (BLVR; EC 1.3.1.24) converts biliverdin into bilirubin, carbon monoxide, and free divalent iron [30]. BLVR has two isozymes: BLVRA and BLVRB. While both isozymes catalyse the reduction of biliverdin to bilirubin, BLVRB produces unconjugated bilirubin, which is usually detectable only for a few weeks after birth. Although BLVRB is still expressed in adulthood, little is known about its function. In contrast, BLVRA is

known to act as a signalling molecule, transcription factor, and has a key role in antioxidant activity [31]. Both isozymes were detected in all brain regions, however, we found only moderate evidence for increased BLVRA in the ENT (Suppl. Table 6; Suppl. Fig. 8). This increase may reflect a compensatory mechanism in response to lowered HMOX-2 levels and subsequently decreased bilirubin expression in the ENT. There was little convincing evidence for differences between cases and controls in terms of light and heavy ferritin chains (Suppl. Table 7; Suppl. Fig. 9), transferrin (Suppl. Table 8; Suppl. Fig. 10), and iron (except for moderate elevation in the hippocampus; Suppl. Table 9; Suppl. Fig. 11).

The presence of elevated haptoglobin and haemopexin throughout the brain in well-characterised cases of sAD without overt signs of brain haemorrhage supports the existence of a microvasculopathy that is pervasive in the brain in most if not all cases of sAD. How generalizable our findings are remains to be determined. Although the Bayesian analysis we employed provides robust evidence that the results are strongly supported within the population studied, it will be necessary for further studies to be performed before the generalisability of these findings can be confirmed. Furthermore, although systemic haptoglobin and haemopexin levels are unlikely to have contributed to the elevated cerebral-protein levels observed here, it cannot be completely excluded.

The evidence here is consistent with the presence of an occult microvasculopathy sufficient to permit the slow leakage of red blood cells through the walls of cerebral microvessels such as capillaries, with consequent haemolysis and generation of free haemoglobin/haeme that in turn stimulate the elevated production of haptoglobin and haemopexin to defend against the toxicity that would otherwise ensue.

Recognised pathogenic processes associated with microvasculopathy and microhaemorrhage in the sAD context include CAA and arteriosclerosis/LH [1,32] so these may, at least in part, be responsible for our current observations. Additionally, recent data show that cases of sAD display widespread elevations in the brain content of free glucose [6-9], which can rise to levels that can exert toxic effects on the microvasculature and cause endothelial dysfunction in contexts such as diabetes mellitus [28,33].

These data taken together with our current findings are consistent with the potential occurrence in sAD of a glucose-driven microvasculopathy similar to that which occurs in diabetes [28]. We postulate that leakiness of the BBB in sAD might reflect, at least in part, a diabetes-like microvasculopathy in addition to CAA and arteriosclerosis/LH. Future studies that probe the presence of diabetes-like vascular perturbations in sAD are warranted.

In a general population where the main cause of new-onset dementia was sAD, a high microbleed count was associated with increased risk of cognitive deterioration and dementia, indicating that microbleeds mark the presence of diffuse vascular and neurodegenerative brain damage [34]. Our current proteomic study of the human brain in sAD is consistent with the concurrence of such "diffuse vascular and neurodegenerative brain damage" [34], coupled with our findings of robust elevations in cerebral haptoglobin and haemopexin levels in multiple representative brain regions. Thus, defective brain-haeme metabolism is identified as a likely mechanism implicated in this symptom complex.

These findings may also help to explain, at least in part, the widespread cerebral inflammation that is frequently reported in AD, given in particular the known, strong proinflammatory actions of free haemoglobin and free haeme.

Declaration of competing interest

The authors have no competing interests with respect to this work. Sponsors had no role in the study design; collection, analysis, or interpretation of data; writing of the manuscript; or decision to submit the article for publication. This work was generated during previous employment of JX, and not during current employment.

Acknowledgements

We thank Cynthia Tse, University of Auckland for management of the research, for proof-reading and submission of the manuscript. We would also like to thank David Eisner and Stuart Allen for proof-reading this manuscript.

We acknowledge the following funding sources: Endocore Research Trust (NZ) (60187); the Lee Trust (NZ); Oakley Mental Health Research Foundation (NZ) (3456030; 3627092; 3701339; 3703253; 3702879); Maurice and Phyllis Paykel Trust (3627036); UKRI Medical Research Council (MR/N0284457/1); NZ Ministry of Business, Innovation & Employment (UOAX0815); The University of Manchester; Northwest Regional Development Agency through a combined programme grant to CADET; and facilitation by the Greater Manchester Comprehensive Local Research Network.

We particularly thank the families of cases with Alzheimer's disease and controls, who so generously supported this research through the donation of brain tissue to the New Zealand Neurological Foundation Human Brain Bank.

Contributions

SAP interpreted the data and wrote the manuscript; JX performed research, analysed data, read and revised the manuscript; RDU performed research, developed the Bayesian data analysis, analysed data, read and revised the manuscript; AWD developed the Bayesian data analysis, read and revised the manuscript; GJSC conceived the study idea, interpreted the data, wrote the manuscript, and bears overall responsibility for the integrity of this manuscript and of the study.

Appendix A. Supplementary material

Supplementary material can be found online.

References

[1] D.R. Thal, E. Ghebremedhin, M. Orantes, et al., Vascular pathology in Alzheimer disease: correlation of cerebral amyloid angiopathy and arteriosclerosis/lipohyalinosis with cognitive decline, J Neuropathol Exp Neurol 62 (2003) 1287-1301.

[2] K. Blennow, M.J. de Leon, H. Zetterberg, Alzheimer's disease, Lancet 368 (2006) 387-403.

[3] K.Y. Chan, W. Wang, J.J. Wu, et al., Epidemiology of Alzheimer's disease and other forms of dementia in China, 1990-2010: a systematic review and analysis, Lancet 381 (2013) 2016-2023.

[4] M. Citron, Alzheimer's disease: strategies for disease modification, Nat Rev Drug Discov 9 (2010) 387-398. 10.1038/nrd2896.

[5] J.L. Cummings, 2-deoxy-2-[^{18}F]-fluoro-D-glucose positron emission tomography in Alzheimer's diagnosis: time for technology transfer, Mol Imaging Biol 4 (2003) 385-386.

[6] J. Xu, P. Begley, S.J. Church, et al., Elevation of brain glucose and polyol-pathway intermediates with accompanying brain-copper deficiency in patients with Alzheimer's disease: metabolic basis for dementia, Sci Rep 6 (2016) 27524.

[7] Y. An, V.R. Varma, S. Varma, et al., Evidence for brain glucose dysregulation in Alzheimer's disease, Alzheimers Dement 14 (2018) 318-329.

[8] R. Mullins, D. Reiter, D. Kapogiannis, Magnetic resonance spectroscopy reveals abnormalities of glucose metabolism in the Alzheimer's brain, Ann Clin Transl Neurol 5 (2018) 262–272.

[9] J. Xu, P. Begley, S.J. Church, et al., Graded perturbations of metabolism in multiple regions of human brain in Alzheimer's disease: Snapshot of a pervasive metabolic disorder, Biochim Biophys Acta 1862 (2016) 1084-1092.

[10] K. Talbot, H.-Y. Wang, H. Kazi, et al., Demonstrated brain insulin resistance in Alzheimer's disease patients is associated with IGF-1 resistance, IRS-1 dysregulation, and cognitive decline, J Clin Invest 122 (2012) 1-23.

[11] J. Xu, S. Patassini, P. Begley, et al., Cerebral deficiency of vitamin B5 (D-pantothenic acid; pantothenate) as a potentially-reversible cause of neurodegeneration and dementia in sporadic Alzheimer's disease, Biochem Biophys Res Commun 527 (2020) 676-681.

[12] J. Cummings, G. Lee, A. Ritter, et al., Alzheimer's disease drug development pipeline: 2019, Alzheimers Dement 5 (2019) 272-229.

[13] I. Alafuzoff, D.R. Thal, T. Arzberger, et al., Assessment of beta-amyloid deposits in human brain: a study of the BrainNet Europe Consortium, Acta Neuropathol 117 (2009) 309-320. 10.1007/s00401-009-0485-4.

[14] C. Duyckaerts, B. Delatour, M.C. Potier, Classification and basic pathology of Alzheimer disease, Acta Neuropathol 118 (2009) 5-36. 10.1007/s00401-009-0532-1.

[15] L.J. Launer, H. Petrovitch, G.W. Ross, et al., AD brain pathology: Vascular origins? Results from the HAAS autopsy study, Neurobiol Aging 29 (2008) 1587–1590.

[16] J. Xu, S. Patassini, N. Rustogi, et al., Regional protein expression in human Alzheimer's brain correlates with disease severity, Commun Biol 2 (2019) 43. https://doi.org/10.1038/s42003-018-0254-9.

[17] H. Braak, E. Braak, Neuropathological stageing of Alzheimer-related changes, Acta Neuropathol 82 (1991) 239-259.

[18] K.A. Jobst, A.D. Smith, M. Szatmari, et al., Rapidly progressing atrophy of medial temporal lobe in Alzheimer's disease, Lancet 343 (1994) 829-830.

[19] S.J. Schönberger, P.F. Edgar, R. Kydd, et al., Proteomic analysis of the brain in Alzheimer's disease: molecular phenotype of a complex disease process, Proteomics 1 (2001) 1519-1528.

[20] O.J. Freeman, R.D. Unwin, A.W. Dowsey, et al., Metabolic dysfunction is restricted to the sciatic nerve in experimental diabetic neuropathy, Diabetes 65 (2016) 228-238.

[21] J. Xu, S.J. Church, S. Patassini, et al., Evidence for widespread, severe brain copper deficiency in Alzheimer's dementia Metallomics 9 (2017) 1106-1119.

[22] S.S. Mirra, A. Heyman, D. McKeel, et al., The Consortium to Establish a Registry for Alzheimer's Disease (CERAD). Part II. Standardization of the neuropathologic assessment of Alzheimer's disease, Neurology 41 (1991) 479-486.

[23] T.J. Montine, C.H. Phelps, T.G. Beach,et al., National Institute on Aging-Alzheimer's Association guidelines for the neuropathologic assessment of Alzheimer's disease: a practical approach, Acta Neuropathol 123 (2012) 1-11.

[24] M. Scholefield, S.J. Church, J. Xu, et al., Evidence that levels of nine essential metals in post-mortem human-Alzheimer's-brain and ex vivo rat-brain tissues are unaffected by differences in post-mortem delay, age, disease staging, and brain bank location, Metallomics 12 (2020) 952-962. DOI: 10.1039/d0mt00048e.

[25] V. Hvidberg, M.B. Maniecki, C. Jacobsen, et al., Identification of the receptor scavenging hemopexin-heme complexes, Blood 106 (2005) 2572-2579. doi: 10.1182/blood-2005-03-1185.

[26] X. Zhao, S. Song, G. Sun, et al., Neuroprotective role of haptoglobin after intracerebral hemorrhage, J Neurosci 29 (2009) 15819-15827. 10.1523/JNEUROSCI.3776-09.2009.

[27] C.M. Morris, J.M. Candy, J.A. Edwardson, et al., Evidence for the localization of haemopexin immunoreactivity in neurones in the human brain, Neurosci Lett 149 (1993) 141-144. 10.1016/0304-3940(93)90756-b.

[28] N. Ashton, Studies of the retinal capillaries in relation to diabetic and other retinopathies, Br J Ophthalmol 47 (1963) 521-538.

[29] M.M. Przybycien-Szymanska, Y. Yang, W.W. Ashley, Microparticle derived proteins as potential biomarkers for cerebral vasospasm post subarachnoid hemorrhage. A preliminary study, Clin Neurol Neurosurg 141 (2016) 48-55. 10.1016/j.clineuro.2015.12.012.

[30] R. Gozzelino, V. Jeney, M.P. Soares, Mechanisms of cell protection by heme oxygenase-1, Annu Rev Pharmacol Toxicol 50 (2010) 323–354.

[31] L. O'Brien, P.A. Hosick, K. John, et al., Biliverdin reductase isozymes in metabolism, Trends Endocrinol Metab 26 (2015) 212-220. 10.1016/j.tem.2015.02.001.

[32] O.A. Selnes, H.V. Vinters, Vascular cognitive impairment, Nat Clin Pract Neurol 2 (2006) 538–547.

[33] J.B. Meigs, C.J. O'Donnell, G.H. Tofler, et al., Hemostatic markers of endothelial dysfunction and risk of incident type 2 diabetes - The Framingham Offspring study, Diabetes 55 (2006) 530-537.

[34] S. Akoudad, F.J. Wolters, A. Viswanathan, et al., Cerebral microbleeds are associated with cognitive decline and dementia: the Rotterdam Study, JAMA Neurol 73 (2016) 934–943.

Figure legends

Fig. 1. Expression of cerebral haptoglobin and haemopexin. Bayesian posterior probability distributions for (**A**) haptoglobin and (**B**) haemopexin for all brain regions. The unique Swiss-Prot IDs for each protein are labelled in brackets. Each plot shows the posterior distribution along with the mean expression ratio and the calculated false-discovery rate (FDR) for each molecule having a up or down-regulation between cases and control of at least 5%.

Tables

Table 1.

Case-control study of post-mortem human brain in Alzheimer's disease: group characteristics.

Variable	Control	Alzheimer's disease
Number	9	9
Age	70.1 (6.7)	70.3 (7.1)
Male sex, n (%)	5 (55.6)	5 (55.6)
PMD (h)	9 (5.5–13.0)	7 (4.0–12.0)
Brain-weight (g)	1260 (1094–1461)	1062 (831-1355)∗
Plaques, n (%)	1 (11)	9 (100)∗∗
Tangles, n (%)	1 (11)	9 (100)∗∗

Values are: age, mean (SD); PMD and brain-weights, median (range): ∗P = 0.005, ∗∗P < 0.0001 compared with corresponding Control value; all other differences are non-significant.

Abbreviation: PMD, *post-mortem* delay.

Table 2.

Multiregional Bayesian-differential quantification for cerebral haptoglobin and haemopexin expression.

Haptoglobin						
Brain region	Peptides	Spectra	Log_2 (fc)	Lower	Upper	Local FDR
Hippocampus	14	67	1.293	0.852	1.715	0.0001
Motor Cortex	16	56	1.087	0.578	1.651	0.0014
Sensory Cortex	7	31	0.897	0.549	1.243	0.0003
Cerebellum	14	54	0.928	0.447	1.350	0.0012
Entorhinal Cortex	10	55	1.225	0.710	1.750	0.0001
Cingulate Gyrus	14	82	1.055	0.566	1.574	0.0011
Haemopexin						
Brain region	Peptides	Spectra	Log_2 (fc)	Lower	Upper	Local FDR
Hippocampus	5	11	0.669	0.334	0.993	0.0016
Motor Cortex	4	5	0.627	0.018	1.288	0.0344
Sensory Cortex	4	11	0.499	0.178	0.809	0.0062
Cerebellum	5	12	0.376	-0.073	0.817	0.0763
Entorhinal Cortex	12	31	0.684	0.301	1.089	0.004
Cingulate Gyrus	4	10	0.325	0.065	0.627	0.0262

Abbreviations: fc: mean fold-change; FDR: False-discovery rate; (Lower/Upper): fc 95% credible interval.

Figures

Fig. 1

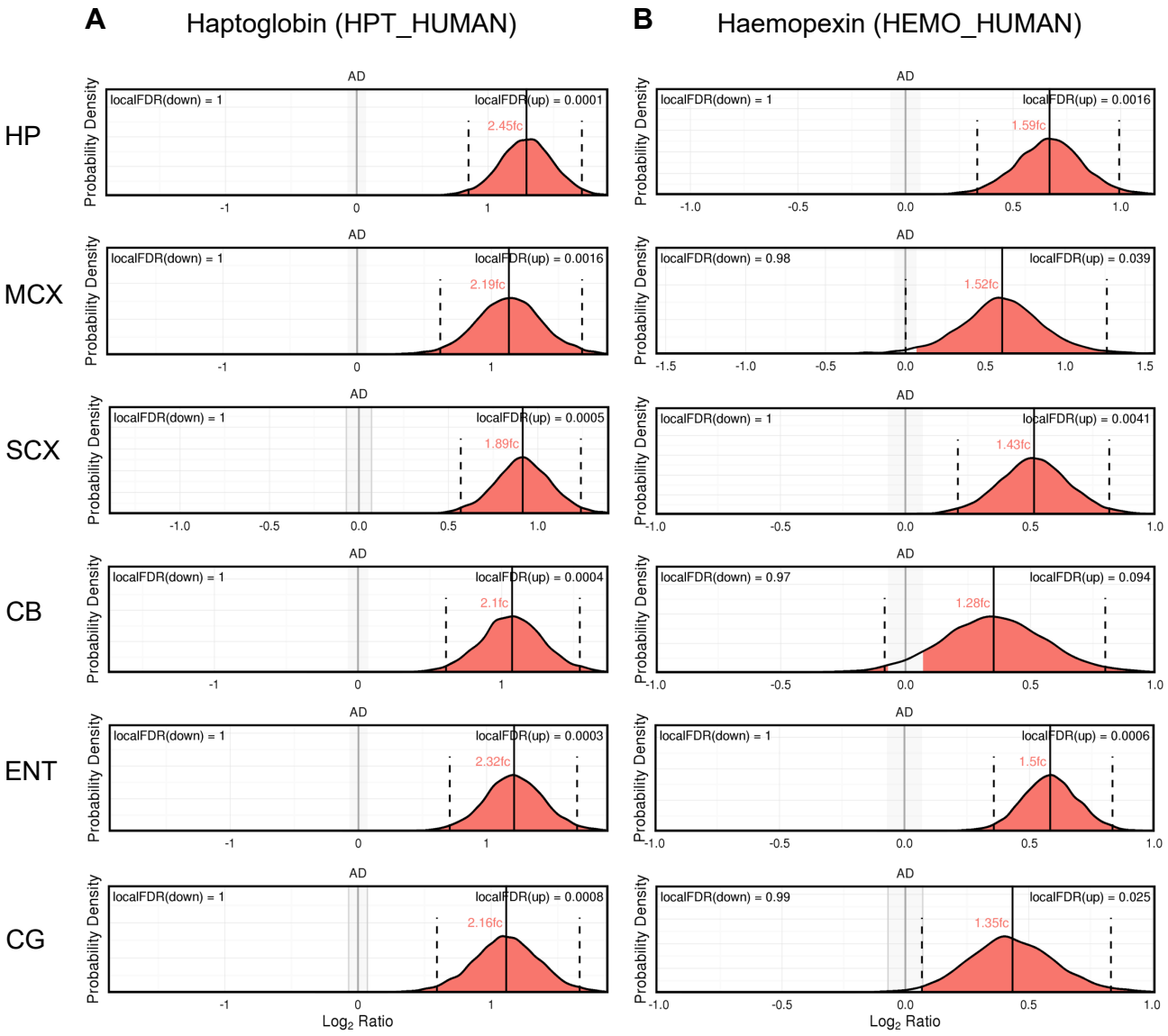

Philbert et al 2020, submission to BBRC of manuscript entitled: "Widespread severe cerebral elevations of haptoglobin and haemopexin in sporadic Alzheimer's disease: evidence for a pervasive microvasculopathy"

Supplementary Material

Supplementary Methods

Supplementary protein extraction and preparation for iTRAQ labelling

Protein extraction and preparation for iTRAQ was carried out according to a previously-described method ([1] and references therein), where each brain region was analysed independently. Brain tissue samples of 100 ± 5 mg were extracted in 500 µL 1M triethylammonium bicarbonate buffer (TEAB) + 0.1% (w/v) sodium dodecyl sulphate (SDS), and homogenised at 25 Hz (2 × 3 min; TissueLyser, Qiagen). Tubes were then vortexed for 10 s and centrifuged at 4 °C (5 min, 13,400 × g). Supernatants were transferred into new tubes and protein concentrations determined (Bradford assay; Bio-Rad Protein Assay Dye Reagent Concentrate) with a plate-reader (SpectraMax M5, Molecular Devices). From each sample, a volume equivalent to 100 µg protein was transferred into a new set of tubes for further processing. Identical reference pool samples (total of 100 µg protein per reference sample) were made by combining portions from four representative individual samples from each group, AD and control. All samples were equalised for final volume using 1 M TEAB + 0.1% (w/v) SDS.

Samples were reduced (0.1 volume of 50 mM dithiothreitol) followed by incubation (60 °C, 30 min). Alkylation was performed by addition of 0.05 volumes of 200 mM iodoacetamide, followed by incubation (dark, room temperature, 10-15 min). Protein digestion was performed overnight (37 °C, 10 µg of modified porcine trypsin, Promega) resuspended in 1M TEAB, ensuring the final SDS concentration fell below 0.05% (w/v). After digestion, the samples were dried completely (Eppendorf concentrator), and re-suspended (30 µL 1M TEAB) to achieve equal volumes across all samples before iTRAQ labelling. The iTRAQ labelling was carried out according to the manufacturer's instructions using the 8-plex iTRAQ kit (AB Sciex). Briefly, vials containing iTRAQ reagent were thawed on the bench for 2-3 min. After pulse centrifugation, 70 µL isopropanol was added to each vial, followed by a further pulse spin. Contents were then transferred to the protein samples and incubated (r.t., 2–3 h). Each 8-plex contained two separate digests of the reference pool sample, three AD samples, and three control samples. iTRAQ-labelled samples destined for the same liquid chromatography/tandem mass spectrometry (LC-MS/MS) run were pooled, then centrifuge (13,400 × g, 5 min). Each pooled sample was then divided into two equal aliquots and dried completely (Eppendorf centrifugal evaporator-concentrator). One pooled aliquot from each 8-plex experiment

was subjected to high-pH reverse phase (HpHRP) for peptide fractionation. Remaining dried-pool aliquots were stored at -80 ^{o}C for repeated analysis if required.

Supplementary data acquisition by low-pH LC-mass spectrometry

The methodology used here was as previously described and is otherwise as presented here in the Suppl. Methods. Each fraction was resuspended in 27 µL of 97% water/3% acetonitrile/0.1% trifluoroacetic acid (TFA; v/v/v) and 9 µL was injected into a nano-Acquity UPLC system (Waters). Peptides were trapped on a nanoACQUITY 2G-V/M Trap Sym C18 5 µm 180 µm × 20 mm (Waters) and washed (flow-rate = 7.5 µL/min, 10 min). Peptides were then eluted and chromatographed using a nanoACQUITY BEH300 C18 1.7 µm 75 µm× 250 mm (Waters) at 300 nL/min using following gradient profile (minutes:%B): 0:3, 3:3, 91:40, 93:90, 108:90, 109:3, 130:3. Buffers used were: buffer A: 97% water + 3% acetonitrile + 0.1% formic acid and buffer B: 100% acetonitrile + 0.1% formic acid (v/v). The eluent was directed into an ESI microionspray II source of a QSTAR Elite Q-TOF spectrometer (AB SCIEX) scanning in MS from 400 to 1200 m/z. Multiply charged peptides (2+ to 4+) were selected for MS/MS analysis (110–1200 m/z). The information-dependent acquisition (IDA) settings were: four precursors per cycle and cycle times (MS 0.75 s, MS/MS1 0.75 s, MS/MS2 0.75 s, MS/MS3 1 s and MS/MS4 1 s). Selected peptides were fragmented twice and then dynamically excluded for 90 s. The resulting data were searched against the human component of the Swissprot database (release 2013_03) using Protein-Pilot v4.0 (AB SCIEX). Search parameters were: iTRAQ 8-plex, trypsin; cys alkylation, iodoacetamide; search effort, thorough. A total of 40,466 proteins were searched. To perform FDR analysis on the protein identification, the search database was reversed and concatenated with the forward database and used as the search DB within ProteinPilot. FDR was determined by calculating the number of reverse 'hits' as a proportion of 'forward' hits using the dedicated worksheet exported from the search software.

Supplementary data processing

Methodologies are generally as previously described [1]. Excerpts from this reference have been reiterated here to support the arguments presented in the main manuscript, quotations in the below text are as designated by inverted commas.

"Bayesian protein-level differential quantification was performed separately for each brain region using v1.0.0 of the in-house developed software BayesProt (https://github.com/biospi/bayesprot/releases/tag/v1.0.0). An earlier version of this technique was presented in Freeman *et al.* [2], which combined Protein-Pilot (AB SCIEX) sample normalisation ('bias correction') with a Bayesian linear mixed-effects model implemented with the MCMCglmm R Package [3]. Analysis of each brain region in isolation adds strength to the comparison of protein expression changes across multiple regions, as these were identified and quantified independently.

Since iTRAQ measurements from Time-of-Flight instruments are recorded as discrete ion counts, and technical/biological variation are assumed log-normal, we adopted a generalised linear mixed model (GLMM) with Poisson likelihood and log-link, where each protein was modelled separately using peptide measurements unique to that protein. The sample normalisation factors represent the mass spectrometer's exposure to each sample, and hence were included as a fixed offset within the model. The current version of BayesProt additionally:

(i) enables estimation of both biological and digestion variance through the incorporation of multiple digests for a single sample (i.e., the six reference pool digests);

(ii) negates the need for Protein-Pilot normalisation by implementing a two-stage GLMM; and

(iii) provides a simplified Markov Chain Monte Carlo (MCMC) mixing criterion for both stages.

In both stages: (a) for each peptide a separate random digest effect is fitted, which has the effect of weighting each peptide's contribution to the protein-level quantification by its reproducibility across digests; (b) the set of measurement channels within each iTRAQ spectrum are each assigned (i) a baseline fixed effect to account for varying selection/ionisation/fragmentation efficiencies across spectra, and (ii) an independent log-normal residual variance to account for over-dispersion due to background contamination and incorrectly identified spectra. In stage one, we also model the interaction between LC-MS/MS run and iTRAQ channel as a fixed effect, i.e., within each run, we infer the protein-level log ratio between iTRAQ channel 113 and channels 114, 115, 116, 117, 118, 119 and 121. For each channel relative to 113, the result is a set of posterior probability distributions, one for each protein in the study; these are combined to derive a posterior distribution for the median log ratio for each channel relative to 113, which is taken as the inferred sample normalisation factors. To construct the PCA plots (see Suppl. Fig. 1 of reference [1]) the protein-level log ratios for all proteins with measurements across all three 8-plexes were first normalised using the sample normalisation factors. Subsequently, for each protein 'variable', the resulting sample 'observations' were then centred and scaled by the mean standard deviation of their posterior distributions, before final input into the R 'prcomp' function to generate the principal components. In stage two, rather than using point estimates of the normalisation factors as fixed sample offsets, a set of sample fixed effects are fitted, which have prior distributions set to the means and variances of the inferred median log ratio distributions. In addition, in stage two we specify the full experimental design: (a) protein-level differential expression fold change between cases and controls is fitted as a condition fixed effect (with control as baseline); (b) due to unequal biological variance across cases and controls, subject is treated as two random effects, one for control samples and one for cases. Using the inferred posterior distribution of the condition fixed effect, we performed a one-sided significance test on the posterior probability that the mean fold change is either above or below ± 1.05 - i.e., at least a 5%

change from control—denoted as P (1.05 fc). The reciprocal of this posterior probability represents the local FDR (lFDR), the probability that this specific test is a false discovery. In this study, we defined significance using a global FDR threshold of 5%, i.e., the largest set of proteins with an average lFDR ≤ 5% were deemed significant and hence delivered to downstream pathway analysis. The condition fixed effect posterior distributions, FDRs and descriptive statistics (mean slog ratio plus 95% highest posterior density interval) for every protein across all regions are presented online (www.manchester.ac.uk/dementia-proteomesproject). Posterior distributions of per-sample protein quantifications are also presented, derived from the latent variables of the sample random effects.

Residual variances were assigned inverse-Gamma priors, whereas random effects were assigned parameter-expanded Cauchy priors. The model was tested with different prior scale factors to establish that the priors were not informative to the outcome. In stages one and two, the model was run with 10 and 100 MCMC chains per protein, respectively, each chain consisting of 10,000 samples preceded by 3,000 burn-in samples. Mixing was assessed using Warnes & Raftery's MCGibbsit run-length diagnostic, combining the estimate error-bounding approach of Raftery and Lewis with the between-chain variance verses within-chain variance approach of Gelman and Rubin (https://cran.r-project.org/web/packages/mcgibbsit/index.html).

For a protein to be considered quantified sufficiently well to be included in downstream pathway, correlation and comparative analyses, we require identification and quantification from at least three spectra. This quality control is important when making comparisons across datasets as it ensures that only high-quality protein quantitation is taken forward into comparative studies, reducing 'noise'."

Data analysis methodologies were otherwise as described in [1].

Supplementary References

[1] J. Xu, S. Patassini, N. Rustogi, I. Riba-Garcia, B.D. Hale, A.M. Phillips, H. Waldvogel, R. Haines, P. Bradbury, A. Stevens, R.L.M. Faull, A.W. Dowsey, G.J.S. Cooper, R.D. Unwin, Regional protein expression in human Alzheimer's brain correlates with disease severity, Commun Biol 2 (2019) 43. https://doi.org/10.1038/s42003-018-0254-9.

Supplementary Figure Legends

Suppl. Fig. 1. Identification of components of an exemplary Bayesian posterior probability distribution plot.

Suppl. Fig. 2. Bayesian posterior distributions for estimated levels of cerebral haptoglobin in each individual sample in this study.

Suppl. Fig. 3. Bayesian posterior distributions for estimated levels of cerebral haemopexin in each individual sample in this study.

Suppl. Fig. 4. Expression of cerebral haemoglobin subunit alpha, beta, and delta. Bayesian posterior distributions for cerebral haemoglobin subunit alpha (**a**), beta (**b**), and delta (**c**) for all brain regions. Each plot shows the probability distribution along with the most likely mean expression ratio and the calculated local false-discovery rate for each molecule having a differential expression between cases and control of at least 5%.

Suppl. Fig. 5. Expression for cerebral fibrinogen alpha, beta, and gamma chains. Bayesian posterior distributions for fibrinogen (**a**) alpha, (**b**) beta, and (**c**) gamma chains for all brain regions. The unique Swiss-Prot IDs for each protein are labelled in brackets. Each plot shows the probability distribution along with the most likely mean expression ratio and the calculated local false-discovery rate (FDR; 1 - posterior probability of up or down regulation) for each molecule having a differential expression between cases and control of at least 5%.

Suppl. Fig. 6. Expression of cerebral LRP1/CD91. Bayesian posterior distributions for cerebral LRP1/CD91 for all brain regions. Each plot shows the probability distribution along with the most likely mean expression ratio and the calculated local false discovery-rate for each molecule having a differential expression between cases and control of at least 5%.

Suppl. Fig. 7. Expression of cerebral haeme oxygenase 2. Bayesian posterior distributions for cerebral haeme oxygenase 2 for all regions. Each plot shows the probability distribution along with the most likely mean expression ratio and the calculated local false discovery rate for each molecule having a differential expression between cases and control of at least 5%.

Suppl. Fig. 8. Expression of cerebral biliverdin reductase A and B. Bayesian posterior distributions for cerebral biliverdin reductase A and B for all regions. Each plot shows the probability distribution along with the most likely mean expression ratio and the calculated local false discovery rate for each molecule having a differential expression between cases and control of at least 5%.

Suppl. Fig. 9. Expression of cerebral ferritin light and heavy chains. Expression posterior distributions for cerebral ferritin light (**a**) and heavy (**b**) chains for all brain regions. Each plot shows the probability distribution along with the most likely mean expression ratio and the calculated local false-discovery rate for each molecule having a differential expression between cases and control of at least 5%.

Suppl. Fig. 10. Expression of cerebral transferrin. Expression posterior distributions for cerebral transferrin for all brain regions. Each plot shows the probability distribution along with the most likely mean expression ratio and the calculated local false-discovery rate for each molecule having a differential expression between cases and control of at least 5%.

Suppl. Fig. 11. Iron concentrations in six brain regions comapared between AD cases and matched controls. Shown are dry-weight iron concentrations in each region of human *post-mortem* brain tissue from control (red) and AD (green) subjects. Abbreviations: HP: Hippocampus; ENT: Entorhinal cortex; SCX: Sensory cortex; MCX: Motor cortex; CG: Cingulate gyrus; and CB: Cerebellum.

Supplementary Tables

Suppl. Table 1.
Clinical characteristics of AD and control brains used in this study.

Case no	Class	Age/sex	Cause of death	Braak stage	Amyloid load	PMD (h)	Brain weight (g)
1	AD	60/M	Alzheimer's disease	VI	3/3	7	1020
2	AD	62/F	Alzheimer's disease	VI	3/3	6	831
3	AD	63/F	Bronchopneumonia	VI	2/3	7	1080
4	AD	70/F	Lung cancer	V	3/3	7	1044
5	AD	73/M	Gastrointestinal haemorrhage	IV	3/3	4	1287
6	AD	74/F	Metastatic cancer	V	3/3	8.5	1062
7	AD	74/M	Pseudomonas bacteraemia	VI	2/3	12	1355
8	AD	77/M	Myocardial infarction	VI	3/3	4.5	1180
9	AD	80/M	Bronchopneumonia/ pulmonary oedema	V	3/3	5.5	1039
10	Control	61/M	Ischaemic heart disease	-	0	7	1258
11	Control	64/F	Pulmonary embolism	-	0	5.5	1260
12	Control	63/F	Ruptured aorta	-	0	12	1280
13	Control	72/F	Emphysema	-	0	9	1230
14	Control	66/M	Ischaemic heart disease	-	0	9	1461
15	Control	76/F	Metastatic carcinoma	II	3/3[a]	12	1094
16	Control	73/M	Ischaemic heart disease	-	0	13	1315
17	Control	78/M	Ruptured abdominal aortic aneurysm	-	0	7.5	1260
18	Control	78/M	Ruptured myocardial infarction	-	0	12	1416

Brain pathology and amyloid load, were determined using the scoring system based on Braak and Braak staging, where a score out of 3 was determined by a qualified neuropathologist and cause of death was determined at post-mortem examination. [a]Despite being phenotypically healthy, patient 15 was found retrospectively to have post-mortem signs consistent with AD and was described as A3, B1, C1 using the 'ABC' criteria for AD neuropathologic change that incorporates histopathological assessments of Aβ deposits (A), staging of neurofibrillary tangles (B) and scoring of neuritic plaques (C). The corresponding data have been retained in the analysis presented in the article due to the early and asymptomatic nature of this patient.
Abbreviations: AD: Alzheimer's disease; F: female; FDR: False-discovery rate; M: male; PMD: *Post-mortem* delay.

Suppl. Table 2.
Multiregional Bayesian-differential quantification for cerebral haemoglobin subunit alpha, beta, and delta expression.

Haemoglobin subunit alpha						
Brain region	Peptides	Spectra	Log_2 (fc)	Lower	Upper	Local FDR
Hippocampus	16	682	0.259	-0.468	0.943	0.2845
Motor Cortex	13	285	0.234	-0.121	0.593	0.1622
Sensory Cortex	16	621	0.169	-0.348	0.683	0.3427
Cerebellum	19	697	0.121	-0.465	0.753	0.4285
Entorhinal Cortex	19	538	0.417	-0.144	1.017	0.0968
Cingulate Gyrus	15	600	0.369	-0.250	0.954	0.1448
Haemoglobin subunit beta						
Brain region	Peptides	Spectra	Log_2 (fc)	Lower	Upper	Local FDR
Hippocampus	15	373	0.212	-0.401	0.813	0.3
Motor Cortex	14	273	0.251	-0.069	0.573	0.1185
Sensory Cortex	13	315	0.159	-0.317	0.640	0.3412
Cerebellum	15	395	0.096	-0.444	0.671	0.4619
Entorhinal Cortex	17	359	0.421	0.001	0.904	0.0564
Cingulate Gyrus	10	340	0.355	-0.173	0.903	0.1312
Haemoglobin subunit delta						
Brain region	Peptides	Spectra	Log_2 (fc)	Lower	Upper	Local FDR
Hippocampus	5	31	0.274	-0.275	0.811	0.2139
Motor Cortex	6	19	0.120	-0.284	0.496	0.3866
Sensory Cortex	6	42	0.151	-0.250	0.539	0.3308
Cerebellum	6	27	0.114	-0.532	0.754	0.4461
Entorhinal Cortex	6	31	0.475	-0.059	0.998	0.06
Cingulate Gyrus	5	42	0.323	-0.158	0.801	0.1299

Abbreviations: fc: mean fold-change; FDR: False-discovery rate; (Lower/Upper): fc 95% credible interval.

Suppl. Table 3.
Multiregional Bayesian-differential quantification for cerebral fibrinogen alpha, beta, and gamma chain expression.

Fibrinogen alpha chain						
Brain region	Peptides	Spectra	Log_2 (fc)	Lower	Upper	Local FDR
Hippocampus	21	64	0.963	0.362	1.549	0.0044
Motor Cortex	15	33	0.874	0.461	1.304	0.0015
Sensory Cortex	14	50	0.897	0.417	1.416	0.0041
Cerebellum	19	57	0.701	0.084	1.323	0.024
Entorhinal Cortex	23	83	0.872	0.232	1.533	0.0119
Cingulate Gyrus	18	56	0.601	0.173	1.060	0.0122
Fibrinogen beta chain						
Brain region	Peptides	Spectra	Log_2 (fc)	Lower	Upper	Local FDR
Hippocampus	17	59	0.665	0.072	1.273	0.0263
Motor Cortex	12	26	0.601	0.178	0.987	0.0067
Sensory Cortex	16	41	0.559	0.133	0.983	0.0126
Cerebellum	14	49	0.555	0.036	1.047	0.0295
Entorhinal Cortex	15	51	0.741	0.225	1.263	0.0078
Cingulate Gyrus	10	29	0.667	0.133	1.224	0.0165
Fibrinogen gamma chain						
Brain region	Peptides	Spectra	Log_2 (fc)	Lower	Upper	Local FDR
Hippocampus	12	37	0.731	0.179	1.249	0.012
Motor Cortex	5	11	0.800	0.342	1.253	0.0026
Sensory Cortex	9	18	0.497	0.146	0.860	0.0108
Cerebellum	12	27	0.540	0.030	1.082	0.0365
Entorhinal Cortex	11	29	0.800	0.178	1.389	0.0126
Cingulate Gyrus	6	13	0.561	0.031	1.068	0.0307

Abbreviations: fc: mean fold-change; FDR: False-discovery rate; (Lower/Upper): fc 95% credible interval.

Suppl. Table 4.
Multiregional Bayesian-differential quantification for cerebral LRP1/CD91 expression.

Brain region	Peptides	Spectra	Log_2 (fc)	Lower	Upper	Local FDR
Hippocampus	19	43	0.107	-0.050	0.260	0.3002
Motor Cortex	11	13	0.118	-0.101	0.340	0.2984
Sensory Cortex	19	44	0.056	-0.062	0.163	0.6068
Cerebellum	25	53	-0.074	-0.147	0.004	0.4601
Entorhinal Cortex	18	33	0.137	-0.041	0.309	0.2061
Cingulate Gyrus	16	28	0.061	-0.036	0.156	0.5828

Abbreviations: fc: mean fold-change; FDR: False-discovery rate; (Lower/Upper): fc 95% credible interval.

Suppl. Table 5.
Multiregional Bayesian-differential quantification for cerebral haeme oxygenase 2 expression.

Brain region	Peptides	Spectra	Log_2 (fc)	Lower	Upper	Local FDR
Hippocampus	7	20	-0.193	-0.397	0.024	0.1075
Motor Cortex	4	8	0.082	-0.343	0.482	0.4706
Sensory Cortex	4	15	0.000	-0.227	0.221	0.7459
Cerebellum	10	28	-0.113	-0.229	0.007	0.2183
Entorhinal Cortex	9	21	-0.240	-0.448	-0.029	0.05
Cingulate Gyrus	2	7	-0.266	-0.460	-0.089	0.0156

Abbreviations: fc: mean fold-change; FDR: False-discovery rate; (Lower/Upper): fc 95% credible interval.

Suppl. Table 6.
Multiregional Bayesian-differential quantification for cerebral biliverdin reductase A and B.

Biliverdin reductase A						
Brain region	Peptides	Spectra	Log_2 (fc)	Lower	Upper	Local FDR
Hippocampus	8	34	0.040	-0.083	0.173	0.6959
Motor Cortex	8	19	0.114	-0.034	0.268	0.2824
Sensory Cortex	12	46	0.103	-0.005	0.207	0.2550
Cerebellum	12	54	0.100	0.008	0.187	0.2434
Entorhinal Cortex	10	44	0.188	0.047	0.329	0.0451
Cingulate Gyrus	8	29	0.142	0.016	0.265	0.1151
Biliverdin reductase B/flavin reductase						
Brain region	Peptides	Spectra	Log_2 (fc)	Lower	Upper	Local FDR
Hippocampus	8	35	0.145	-0.048	0.347	0.2016
Motor Cortex	7	19	-0.016	-0.217	0.180	0.7224
Sensory Cortex	8	30	-0.064	-0.266	0.129	0.5234
Cerebellum	9	35	0.036	-0.134	0.208	0.6685
Entorhinal Cortex	7	35	0.141	-0.094	0.371	0.2549
Cingulate Gyrus	5	23	0.026	-0.095	0.141	0.7911

Abbreviations: fc: mean fold-change; FDR: False-discovery rate; (Lower/Upper): fc 95% credible interval.

Suppl. Table 7.
Multiregional Bayesian-differential quantification for cerebral ferritin heavy and light chain expression.

Ferritin heavy chain						
Brain region	Peptides	Spectra	Log_2 (fc)	Lower	Upper	Local FDR
Hippocampus	11	59	0.194	-0.047	0.421	0.1308
Motor Cortex	8	23	0.046	-0.262	0.350	0.5641
Sensory Cortex	9	49	0.100	-0.045	0.241	0.3283
Cerebellum	9	46	0.222	-0.196	0.664	0.2209
Entorhinal Cortex	10	63	-0.228	-0.691	0.193	0.2229
Cingulate Gyrus	8	50	0.262	0.004	0.520	0.0695
Ferritin light chain						
Brain region	Peptides	Spectra	Log_2 (fc)	Lower	Upper	Local FDR
Hippocampus	8	36	0.287	0.006	0.545	0.0502
Motor Cortex	6	24	0.045	-0.209	0.297	0.5834
Sensory Cortex	9	27	0.118	0.017	0.218	0.1578
Cerebellum	8	28	0.151	-0.300	0.626	0.3539
Entorhinal Cortex	10	41	0.035	-0.310	0.386	0.5881
Cingulate Gyrus	8	34	0.372	0.023	0.736	0.0444

Abbreviations: fc: mean fold-change; FDR: False-discovery rate; (Lower/Upper): fc 95% credible interval.

Suppl. Table 8.
Multiregional Bayesian-differential quantification for cerebral transferrin expression.

Brain region	Peptides	Spectra	Log_2 (fc)	Lower	Upper	Local FDR
Hippocampus	19	102	-0.024	-0.377	0.358	0.6105
Motor Cortex	23	75	-0.024	-0.448	0.397	0.5978
Sensory Cortex	16	81	-0.028	-0.309	0.230	0.6297
Cerebellum	19	67	0.029	-0.298	0.336	0.6086
Entorhinal Cortex	35	137	-0.175	-0.481	0.171	0.2431
Cingulate Gyrus	26	111	0.080	-0.146	0.294	0.4593

Abbreviations: fc: mean fold-change; FDR: False-discovery rate; (Lower/Upper): fc 95% credible interval.

Suppl. Table 9.
Multiregional iron concentrations in AD and control brains.

Brain region	Control	AD	*P* value
Hippocampus*	3.63 (0.94)	5.87 (1.79)	0.007
Entorhinal cortex*	5.29 (0.998)	5.96 (1.04)	0.199
Cingulate Gyrus	4.89 (1.42)	4.07 (1.82)	0.301
Sensory cortex	5.34 (0.82)	5.80 (0.97)	0.289
Motor cortex	5.95 (0.84)	6.01 (1.17)	0.894
Cerebellum†	6.34 (2.19)	5.93 (3.36)	0.773

Values are means (SD). *P* values for significance of between-group differences were calculated by Welch's t-test based on measurements from AD (n = 9) and control (n = 9) brains.

* Regions had AD (n = 9) and control (n = 8) brains.

† Region had AD (n = 8) and control (n = 9) brains.

Supplementary Figures

Suppl. Fig. 1

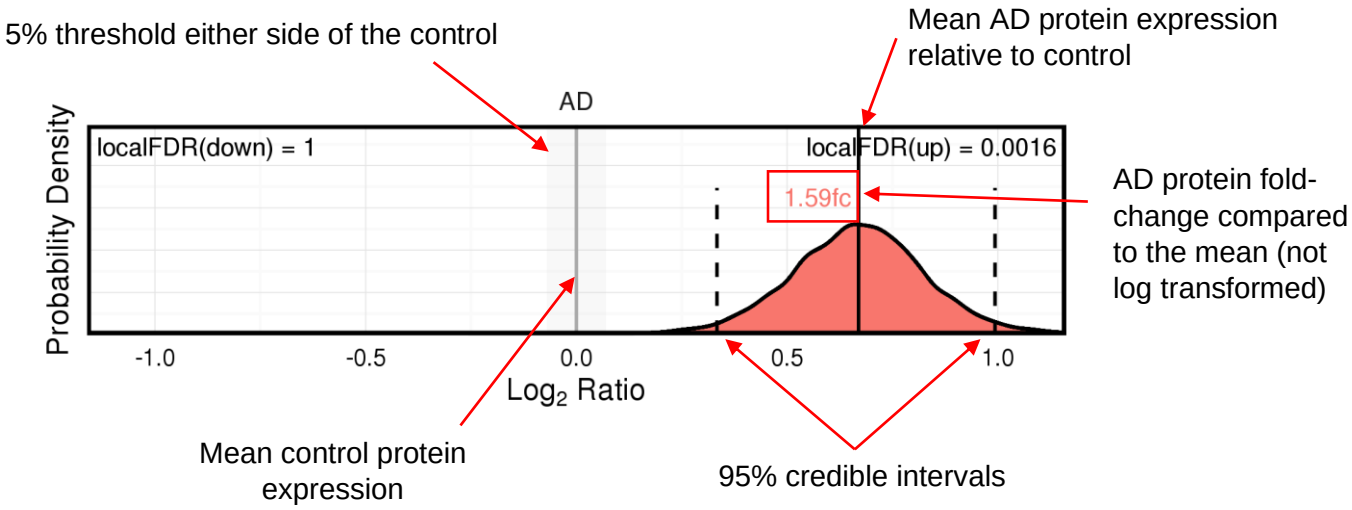

Suppl. Fig. 2

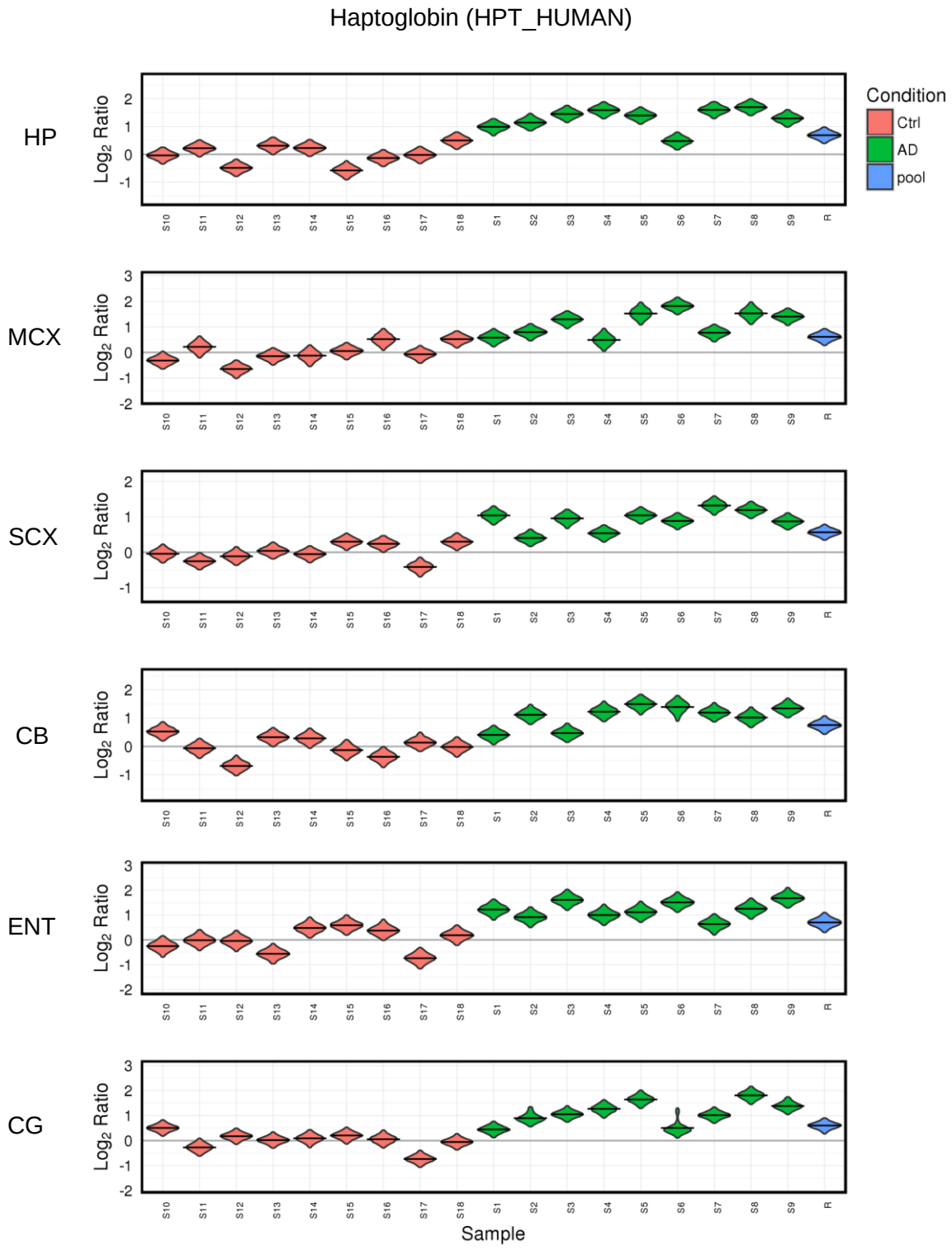
Haptoglobin (HPT_HUMAN)
HP
MCX
SCX
CB
ENT
CG
Log2 Ratio
Condition
Ctrl
AD
pool
S10
S11
S12
S13
S14
S15
S16
S17
S18
S1
S2
S3
S4
S5
S6
S7
S8
S9
R
Sample

Suppl. Fig. 3

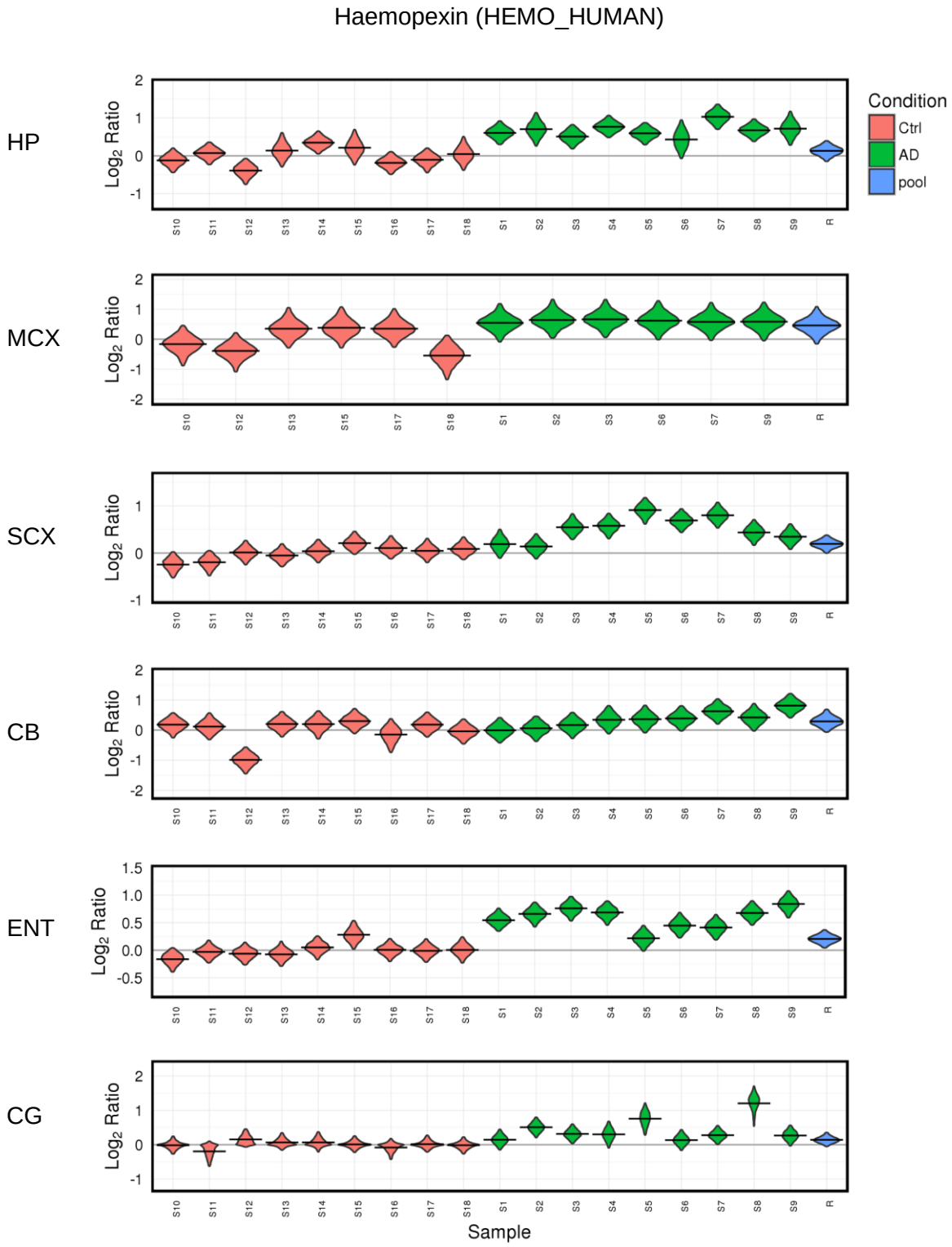
Haemopexin (HEMO_HUMAN)
HP
MCX
SCX
CB
ENT
CG
Log2 Ratio
Condition
Ctrl
AD
pool
S10 S11 S12 S13 S14 S15 S16 S17 S18 S1 S2 S3 S4 S5 S6 S7 S8 S9 R
Sample

Suppl. Fig. 4

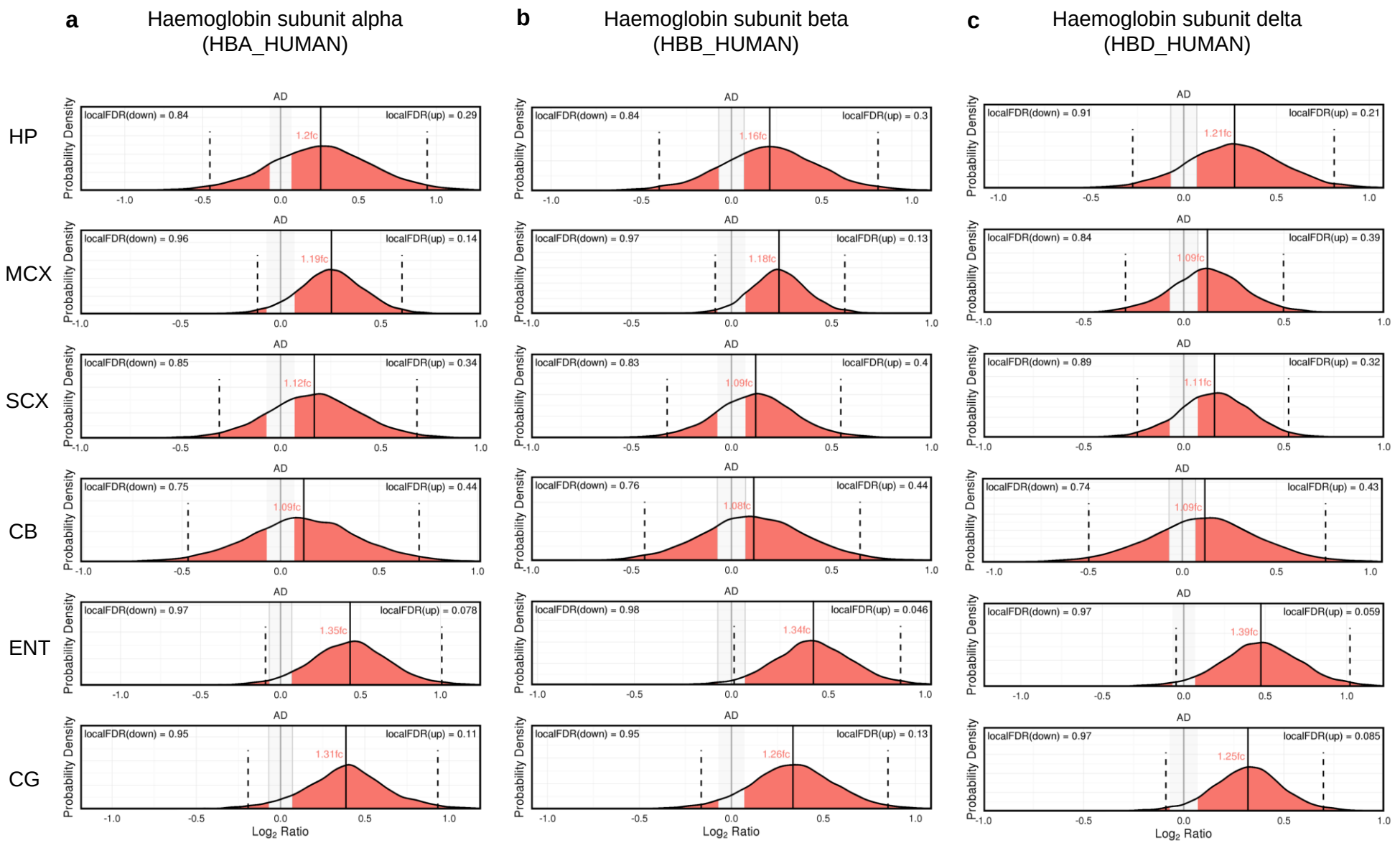
a
Haemoglobin subunit alpha
(HBA_HUMAN)
b
Haemoglobin subunit beta
(HBB_HUMAN)
c
Haemoglobin subunit delta
(HBD_HUMAN)
HP
MCX
SCX
CB
ENT
CG
AD
Probability Density
localFDR(down) = 0.84
localFDR(up) = 0.29
1.2fc
localFDR(down) = 0.84
localFDR(up) = 0.3
1.16fc
localFDR(down) = 0.91
localFDR(up) = 0.21
1.21fc
localFDR(down) = 0.96
localFDR(up) = 0.14
1.19fc
localFDR(down) = 0.97
localFDR(up) = 0.13
1.18fc
localFDR(down) = 0.84
localFDR(up) = 0.39
1.09fc
localFDR(down) = 0.85
localFDR(up) = 0.34
1.12fc
localFDR(down) = 0.83
localFDR(up) = 0.4
1.09fc
localFDR(down) = 0.89
localFDR(up) = 0.32
1.11fc
localFDR(down) = 0.75
localFDR(up) = 0.44
1.09fc
localFDR(down) = 0.76
localFDR(up) = 0.44
1.08fc
localFDR(down) = 0.74
localFDR(up) = 0.43
1.09fc
localFDR(down) = 0.97
localFDR(up) = 0.078
1.35fc
localFDR(down) = 0.98
localFDR(up) = 0.046
1.34fc
localFDR(down) = 0.97
localFDR(up) = 0.059
1.39fc
localFDR(down) = 0.95
localFDR(up) = 0.11
1.31fc
localFDR(down) = 0.95
localFDR(up) = 0.13
1.26fc
localFDR(down) = 0.97
localFDR(up) = 0.085
1.25fc
-1.0
-0.5
0.0
0.5
1.0
Log2 Ratio

Suppl. Fig. 5

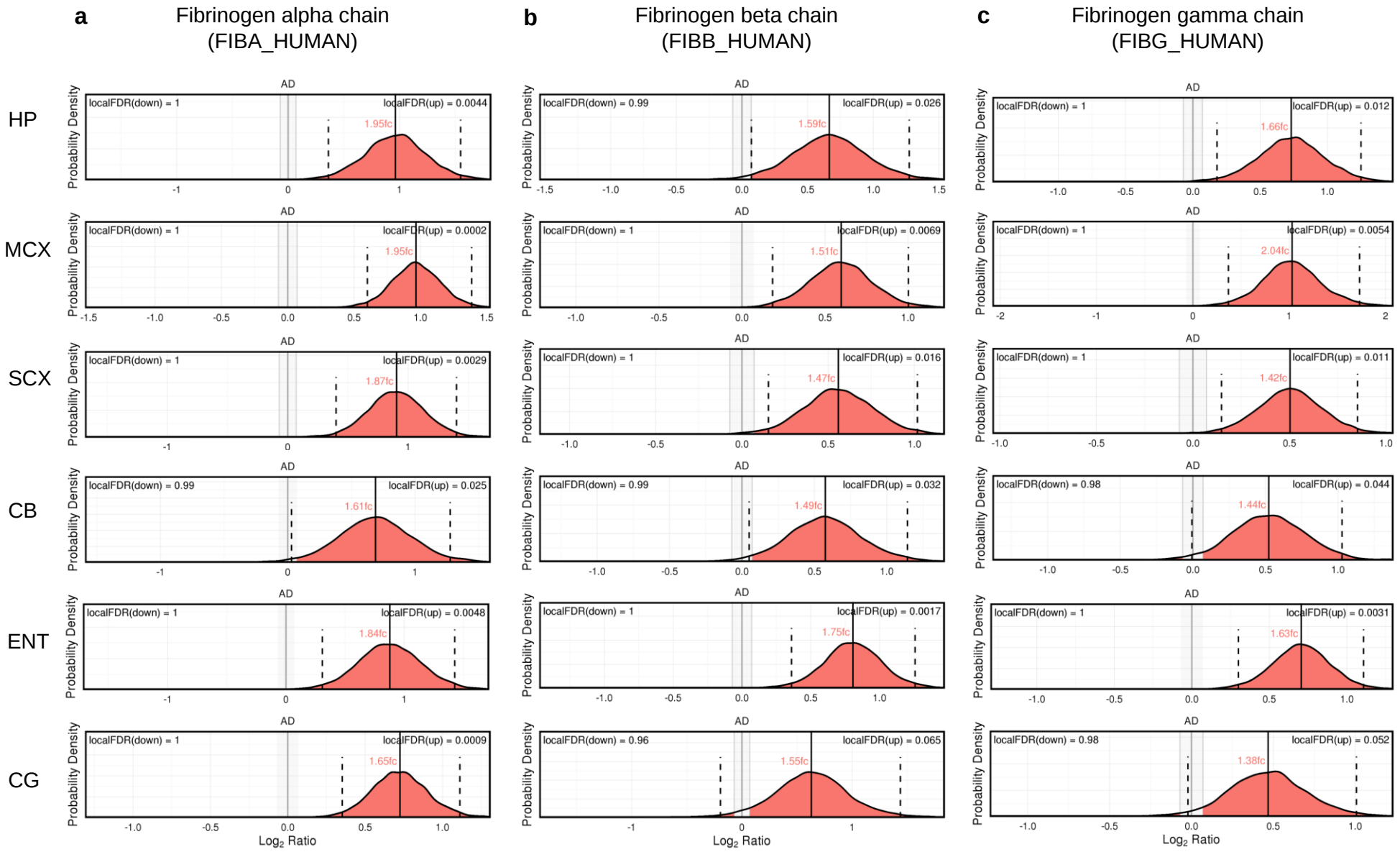
a
Fibrinogen alpha chain
(FIBA_HUMAN)
b
Fibrinogen beta chain
(FIBB_HUMAN)
c
Fibrinogen gamma chain
(FIBG_HUMAN)
HP
MCX
SCX
CB
ENT
CG
AD
Probability Density
localFDR(down) = 1
localFDR(up) = 0.0044
1.95fc
localFDR(down) = 0.99
localFDR(up) = 0.026
1.59fc
localFDR(down) = 1
localFDR(up) = 0.012
1.66fc
localFDR(down) = 1
localFDR(up) = 0.0002
1.95fc
localFDR(down) = 1
localFDR(up) = 0.0069
1.51fc
localFDR(down) = 1
localFDR(up) = 0.0054
2.04fc
localFDR(down) = 1
localFDR(up) = 0.0029
1.87fc
localFDR(down) = 1
localFDR(up) = 0.016
1.47fc
localFDR(down) = 1
localFDR(up) = 0.011
1.42fc
localFDR(down) = 0.99
localFDR(up) = 0.025
1.61fc
localFDR(down) = 0.99
localFDR(up) = 0.032
1.49fc
localFDR(down) = 0.98
localFDR(up) = 0.044
1.44fc
localFDR(down) = 1
localFDR(up) = 0.0048
1.84fc
localFDR(down) = 1
localFDR(up) = 0.0017
1.75fc
localFDR(down) = 1
localFDR(up) = 0.0031
1.63fc
localFDR(down) = 1
localFDR(up) = 0.0009
1.65fc
localFDR(down) = 0.96
localFDR(up) = 0.065
1.55fc
localFDR(down) = 0.98
localFDR(up) = 0.052
1.38fc
Log2 Ratio

Suppl. Fig. 6

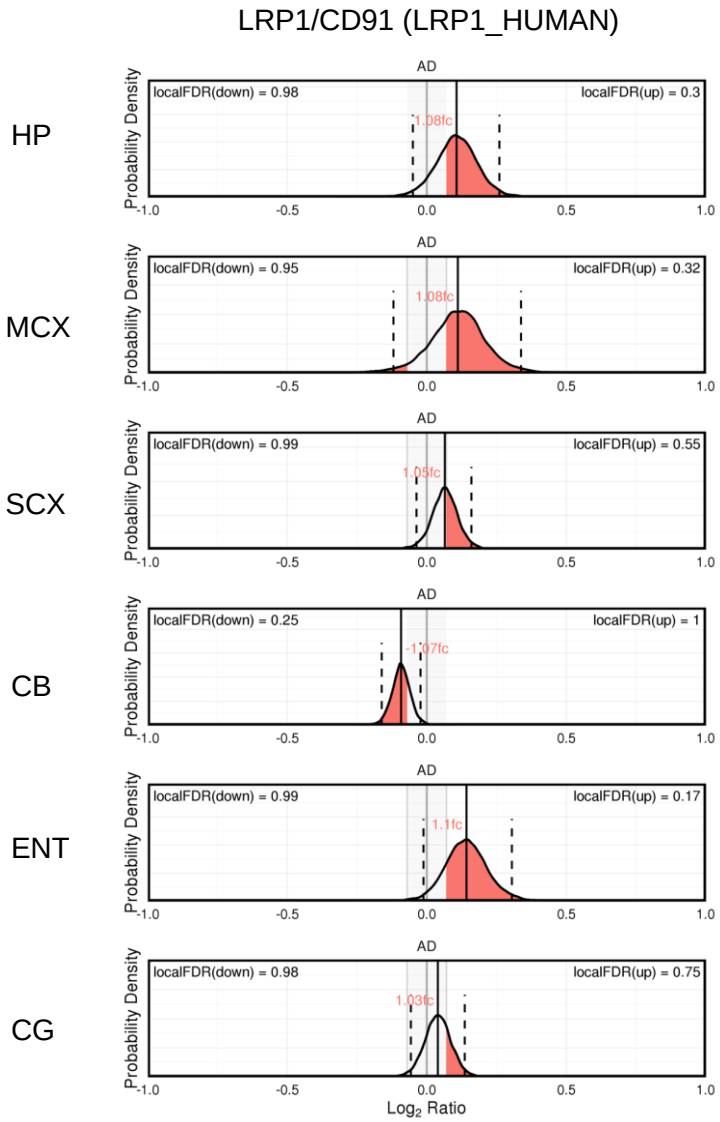
LRP1/CD91 (LRP1_HUMAN)
HP
MCX
SCX
CB
ENT
CG
AD
localFDR(down) = 0.98
localFDR(up) = 0.3
1.08fc
localFDR(down) = 0.95
localFDR(up) = 0.32
1.08fc
localFDR(down) = 0.99
localFDR(up) = 0.55
1.05fc
localFDR(down) = 0.25
localFDR(up) = 1
-1.07fc
localFDR(down) = 0.99
localFDR(up) = 0.17
1.1fc
localFDR(down) = 0.98
localFDR(up) = 0.75
1.03fc
Probability Density
-1.0
-0.5
0.0
0.5
1.0
Log2 Ratio

Suppl. Fig. 7

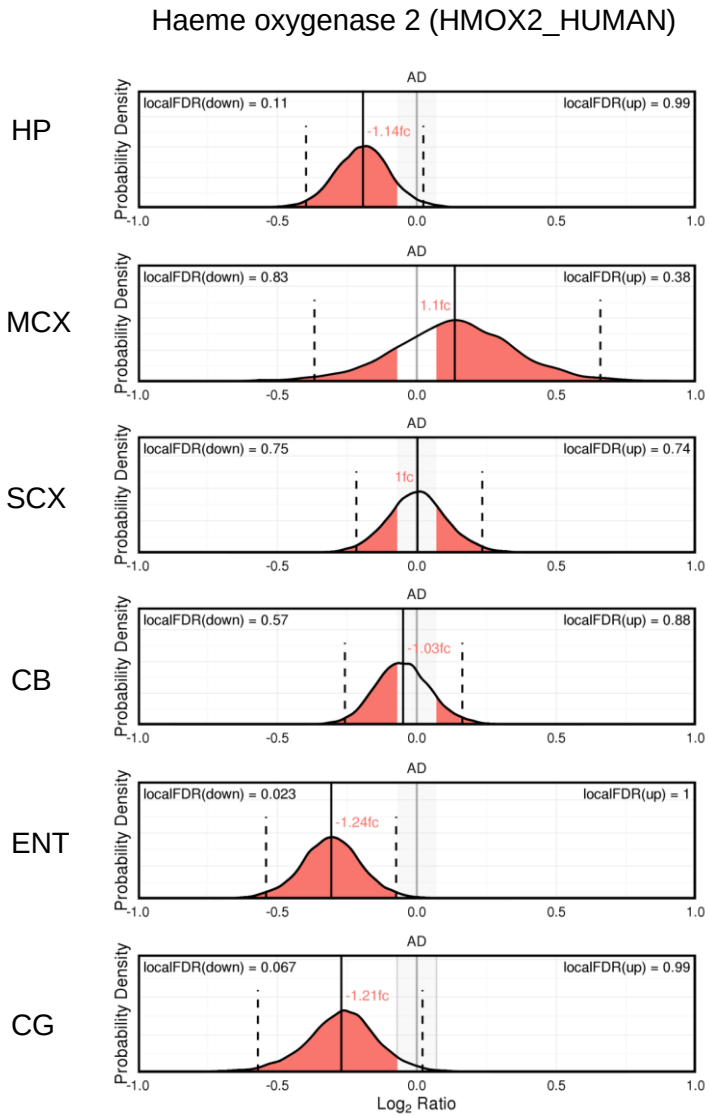
Haeme oxygenase 2 (HMOX2_HUMAN)
HP
MCX
SCX
CB
ENT
CG
AD
Probability Density
localFDR(down) = 0.11
localFDR(up) = 0.99
-1.14fc
localFDR(down) = 0.83
localFDR(up) = 0.38
1.1fc
localFDR(down) = 0.75
localFDR(up) = 0.74
1fc
localFDR(down) = 0.57
localFDR(up) = 0.88
-1.03fc
localFDR(down) = 0.023
localFDR(up) = 1
-1.24fc
localFDR(down) = 0.067
localFDR(up) = 0.99
-1.21fc
-1.0
-0.5
0.0
0.5
1.0
Log2 Ratio

Suppl. Fig 8

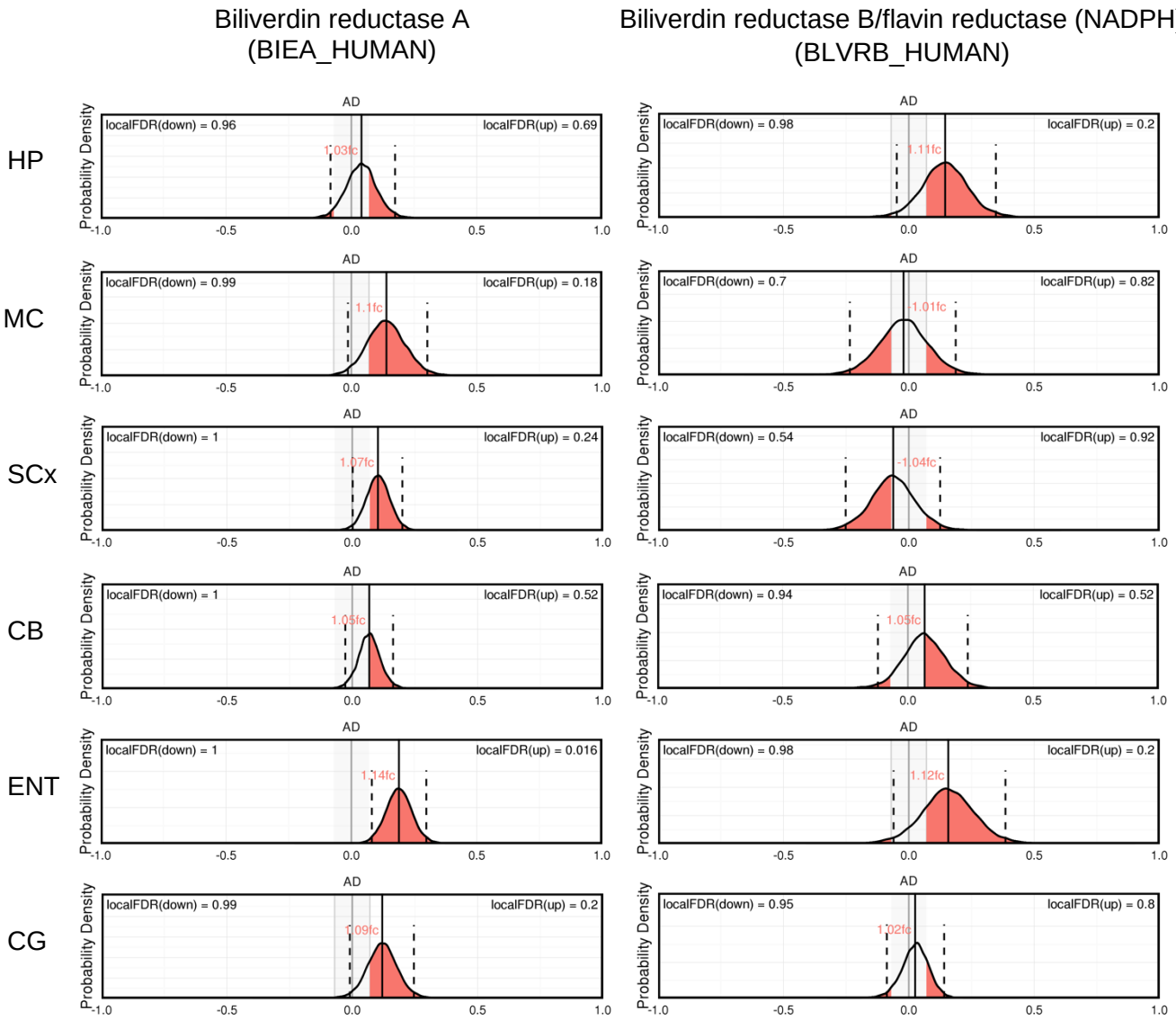
Biliverdin reductase A
(BIEA_HUMAN)
Biliverdin reductase B/flavin reductase (NADPH)
(BLVRB_HUMAN)
HP
MC
SCx
CB
ENT
CG
AD
Probability Density
localFDR(down) = 0.96
localFDR(up) = 0.69
1.03fc
localFDR(down) = 0.98
localFDR(up) = 0.2
1.11fc
localFDR(down) = 0.99
localFDR(up) = 0.18
1.1fc
localFDR(down) = 0.7
localFDR(up) = 0.82
-1.01fc
localFDR(down) = 1
localFDR(up) = 0.24
1.07fc
localFDR(down) = 0.54
localFDR(up) = 0.92
-1.04fc
localFDR(down) = 1
localFDR(up) = 0.52
1.05fc
localFDR(down) = 0.94
localFDR(up) = 0.52
1.05fc
localFDR(down) = 1
localFDR(up) = 0.016
1.14fc
localFDR(down) = 0.98
localFDR(up) = 0.2
1.12fc
localFDR(down) = 0.99
localFDR(up) = 0.2
1.09fc
localFDR(down) = 0.95
localFDR(up) = 0.8
1.02fc
-1.0
-0.5
0.0
0.5
1.0

Suppl. Fig. 9

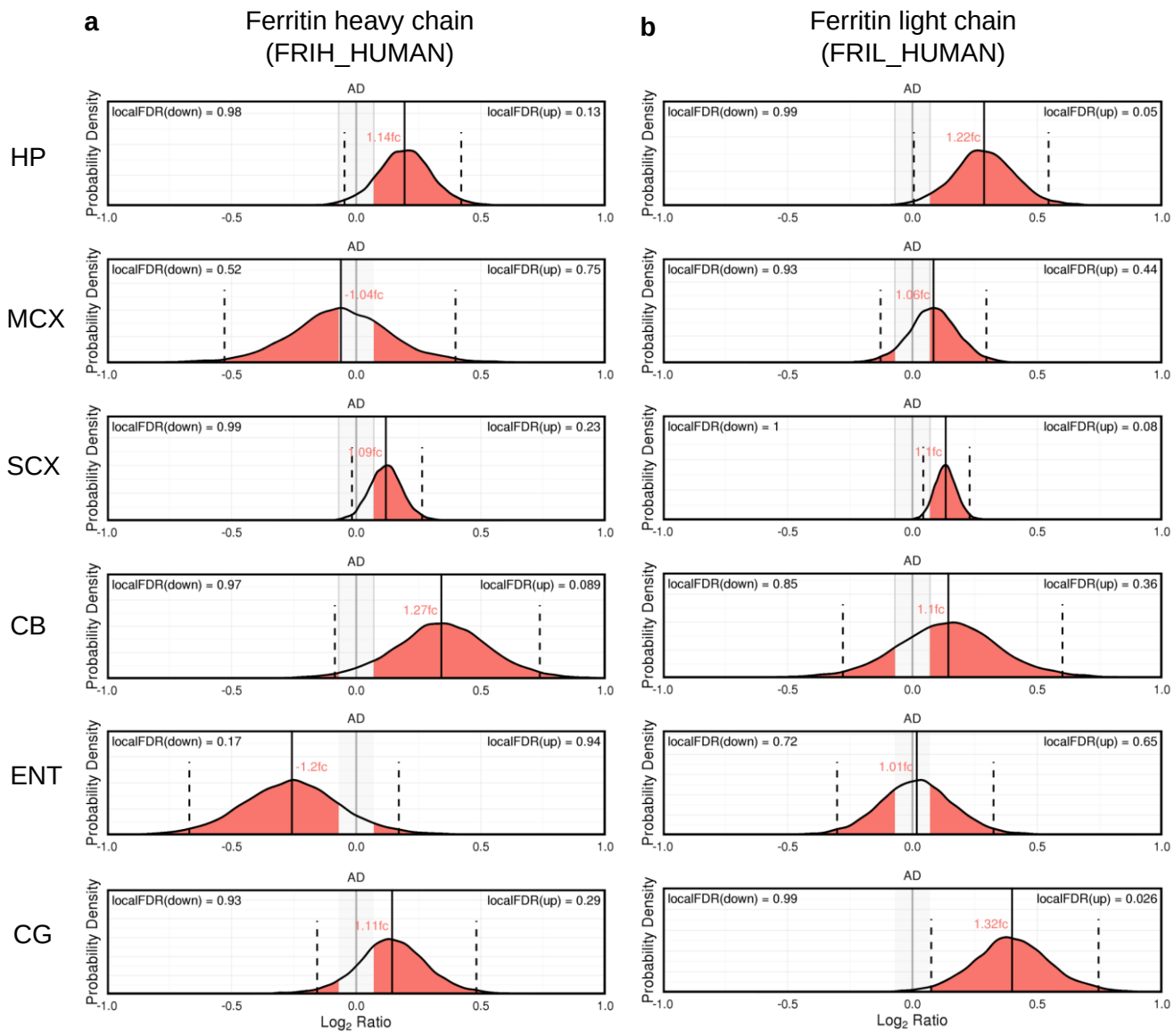
a
Ferritin heavy chain
(FRIH_HUMAN)
b
Ferritin light chain
(FRIL_HUMAN)
HP
MCX
SCX
CB
ENT
CG
AD
Probability Density
localFDR(down) = 0.98
localFDR(up) = 0.13
1.14fc
localFDR(down) = 0.99
localFDR(up) = 0.05
1.22fc
localFDR(down) = 0.52
localFDR(up) = 0.75
-1.04fc
localFDR(down) = 0.93
localFDR(up) = 0.44
1.06fc
localFDR(down) = 0.99
localFDR(up) = 0.23
1.09fc
localFDR(down) = 1
localFDR(up) = 0.08
1.1fc
localFDR(down) = 0.97
localFDR(up) = 0.089
1.27fc
localFDR(down) = 0.85
localFDR(up) = 0.36
1.1fc
localFDR(down) = 0.17
localFDR(up) = 0.94
-1.2fc
localFDR(down) = 0.72
localFDR(up) = 0.65
1.01fc
localFDR(down) = 0.93
localFDR(up) = 0.29
1.11fc
localFDR(down) = 0.99
localFDR(up) = 0.026
1.32fc
-1.0
-0.5
0.0
0.5
1.0
Log2 Ratio

Suppl. Fig. 10

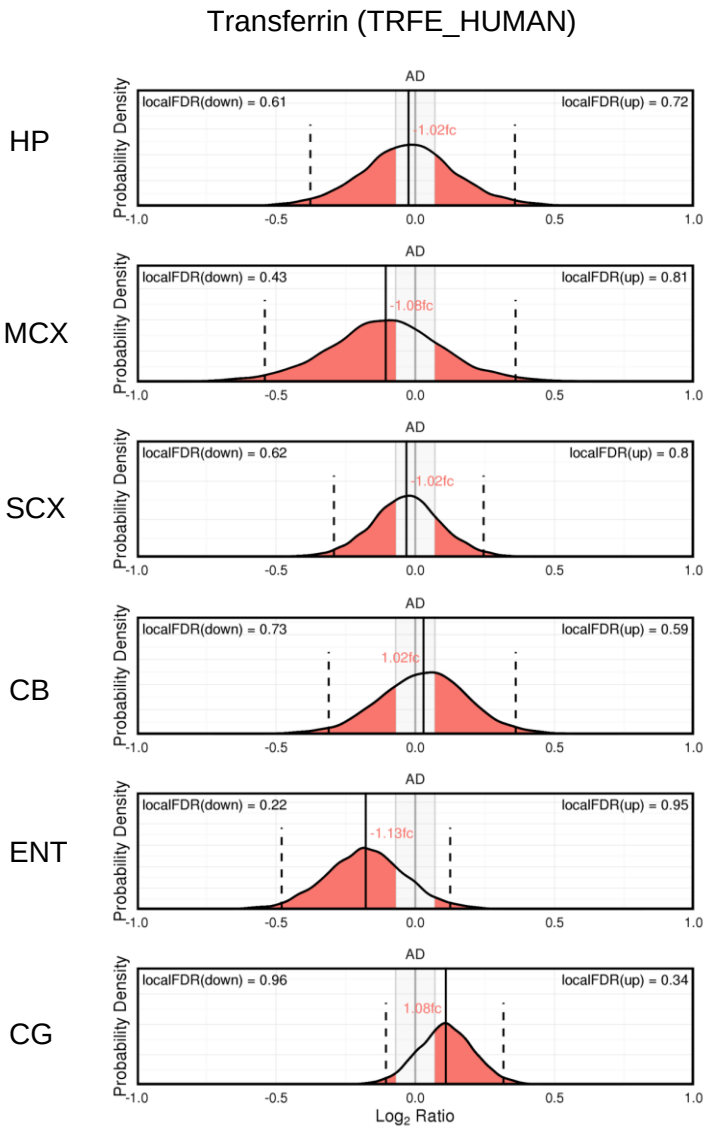
Transferrin (TRFE_HUMAN)
HP
MCX
SCX
CB
ENT
CG
AD
localFDR(down) = 0.61
localFDR(up) = 0.72
1.02fc
localFDR(down) = 0.43
localFDR(up) = 0.81
-1.08fc
localFDR(down) = 0.62
localFDR(up) = 0.8
-1.02fc
localFDR(down) = 0.73
localFDR(up) = 0.59
1.02fc
localFDR(down) = 0.22
localFDR(up) = 0.95
-1.13fc
localFDR(down) = 0.96
localFDR(up) = 0.34
1.08fc
Probability Density
-1.0
-0.5
0.0
0.5
1.0
Log2 Ratio

Suppl. Fig. 11

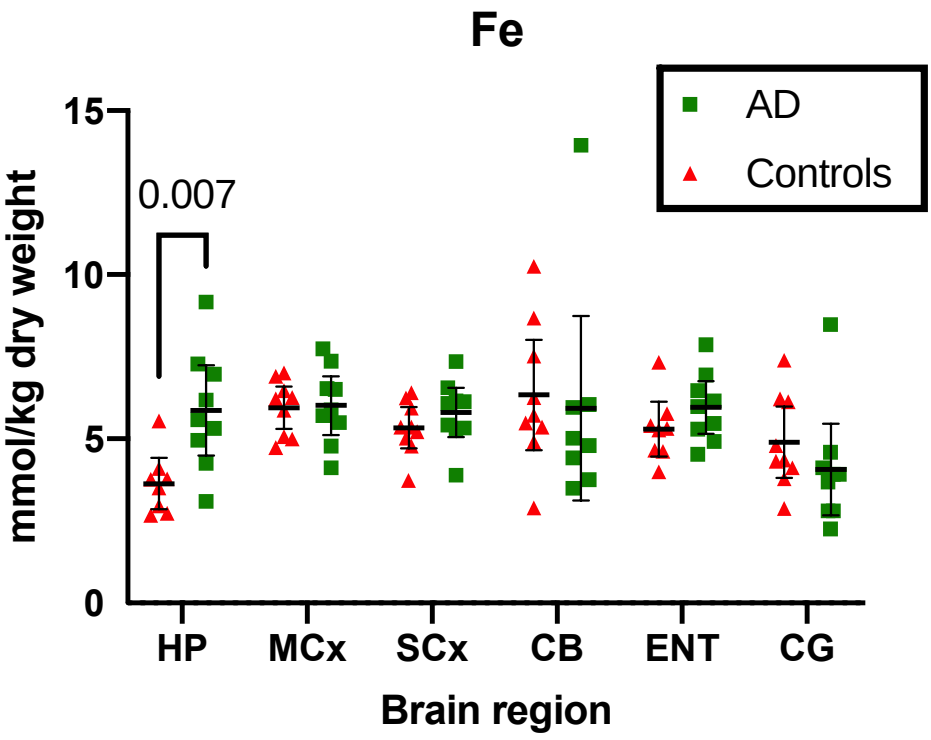
Fe
AD
Controls
0.007
15
10
5
0
mmol/kg dry weight
HP
MCx
SCx
CB
ENT
CG
Brain region